Chaos, Solitons and Fractals 83 (2016) 140–146

Contents lists available at ScienceDirect

Chaos, Solitons and Fractals

Nonlinear Science, and Nonequilibrium and Complex Phenomena

journal homepage: www.elsevier.com/locate/chaos

Stability of a spatial model of social interactions

Jean Bragard [a,*], Pascal Mossay [b,c]

[a] Department of Physics & Applied Mathematics, University of Navarra, Pamplona E-31080, Spain
[b] Newcastle University, 5 Barrack Road, Newcastle, NE1 4SE, UK
[c] CORE, 34 Voie du Roman Pays, 1348 Louvain-la-Neuve, Belgium

ARTICLE INFO

Article history:
Received 24 April 2015
Accepted 29 November 2015
Available online 29 December 2015

Keywords:
Spatial economy
Social interactions
Stability of equilibrium
Nonlinear methods

ABSTRACT

We study a spatial model of social interactions. Though the properties of the spatial equilibrium have been largely discussed in the existing literature, the stability of equilibrium remains an unaddressed issue. Our aim is to fill up this gap by introducing dynamics in the model and by determining the stability of equilibrium. First we derive a variational equation useful for the stability analysis. This allows to study the corresponding eigenvalue problem. While odd modes are shown to be always stable, there is a single even mode of which stability depends on the model parameters. Finally various numerical simulations illustrate our theoretical results.

1. Introduction

The economic literature on spatial agglomerations has been emphasizing the role of increasing returns in the production sector as favoring the spatial clustering of economic activities, see [1]. However, it is known that both market and non-market forces play an important role in determining the balance between agglomeration and dispersion forces in a spatial economy. In particular, social interactions through face-to-face contacts also contribute to the gathering of individuals in villages, agglomerations, or cities, see [2]. Beckmann [3] introduced social interactions into a land market model. In his model, the spatial equilibrium structure results from the interplay between the agglomeration force generated by social interactions and the dispersion force channeled by land prices. Beckmann's work has been revisited by Fujita and Thisse [4], Mossay and Picard [5], and Blanchet et al. [6] by studying further the properties of the spatial equilibrium. In particular, Mossay and Picard [5] have shown that Beckmann's equilibrium along a segment is unique and have extended the analysis along a circle. Blanchet et al. [6] have extended Beckmann's framework so as to encompass general agents' preferences: along a segment, the uniqueness of spatial equilibrium holds for a large class of utility functions. Though the static aspects of Beckmann's framework have been largely studied, dynamic aspects of the model have not received attention yet. The purpose of this paper is to study the stability of spatial equilibrium in Beckmann's model, an issue which is left unaddressed in the existing literature.

First, we extend the spatial model of social interactions by Mossay and Picard [5] to a dynamic setting accounting for the fact that individuals tend to relocate to locations providing them with higher utility levels. This leads to an integro-differential equation governing the evolution of the population distribution over space and time. In the New Economic Geography literature (see e.g. [1]), most models are often discrete and usually involve a small number of locations. In that case, stability methods require the study of a finite number of eigenvalues (e.g. [7,8]). In that literature, dynamic models set in continuous space, as is the case here, are rare. The few existing studies rely on the method of normal modes to analyze stability; e.g. [1,9,10] or [11]. In contrast here, we derive a variational equation for stability, and only then study the even and odd modes of the eigenvalue problem.

* Corresponding author. Tel.: +34 948425600; fax: +34 948425740.
E-mail addresses: jbragard@unav.es (J. Bragard), pascal.mossay@ncl.ac.uk (P. Mossay).

http://dx.doi.org/10.1016/j.chaos.2015.11.040
0960-0779/

Second, we present various numerical simulations illustrating our theoretical results. For this purpose we perform simulations for stable and unstable parameter configurations as well as for various initial conditions such as uniform random noise or multiple-center configurations.

Section 2 provides the dynamic extension of the model. The stability analysis is presented in Section 3. In Section 4, numerical simulations are performed and explained. Section 5 concludes.

2. The spatial model of social interactions

Our model builds on the spatial model of social interactions by Mossay and Picard [5], and Blanchet et al. [6] along a line segment. Let us denote the density of agents in location x at time t by $\lambda(x, t)$. Agents benefit from social contacts with other agents. In order to establish those contacts, agents have to travel along the segment. The social utility that an agent in location x derives from interacting with other agents is given by

$$S(x,t) = \alpha \int \lambda(y,t)\, dy - \tau \int |x-y|\, \lambda(y,t)\, dy \tag{1}$$

where the first integral describes the social interactions with other agents with $\alpha > 0$ and the second one accounts for the traveling cost incurred to meet them with $\tau > 0$. The utility $V(x, t)$ of agents consists of the social utility minus a disutility resulting from congestion

$$V(x,t) = S(x,t) - \beta\, \lambda(x,t) \tag{2}$$

where $\beta\lambda(x, t)$ is the congestion cost with $\beta > 0$. In [5], the congestion cost results from congestion in the land market: higher agent densities lead to higher land prices, which translates into a disutility. In that paper, the agents' preference for land is chosen so that the resulting congestion cost is linear in λ, which is the functional form we also retain in this paper.

We now extend the static framework established by Mossay and Picard to a dynamic setting. In our model, agents tend to relocate towards locations providing them with higher utilities:

$$\frac{\partial \lambda}{\partial t} = k\,[V(x,t) - \bar{V}(t)]\,\lambda(x,t) \tag{3}$$

where $\bar{V}(t)$ denotes the first spatial moment of the utility, $\int \lambda(y, t)V(y, t)\, dy$, and $k > 0$ a mobility parameter.

2.1. Invariant manifold

By integrating Eq. (3) over the whole domain and by denoting :

$$I = \int \lambda(y,t)\, dy\,, \tag{4}$$

we obtain the following equation for I:

$$\frac{dI}{dt} = k\bar{V}(t)\,[1-I]\,, \tag{5}$$

we see that $I = 1$ is an invariant manifold associated with the dynamics given by Eq. (3). The transverse stability of this manifold is given by the sign of $\bar{V}$. If $\bar{V} > 0$ the manifold is locally stable. We will return to this point latter.

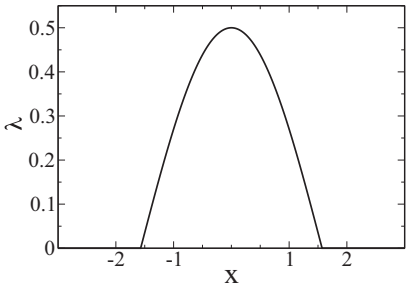

Fig. 1. Steady solution $\lambda^{(s)}(x)$ for $\alpha = 1$, $\beta = 2$ and $\tau = 1$ such that $\delta = 1$ and $b = \pi/2$.

2.2. Steady-state solution

Let us now look for a steady-state solution to Eq. (3). If such a solution exists it satisfies:

$$V(x,t) = \bar{V}(t) = \text{constant} \tag{6}$$

or equivalently

$$\tau \int |x-y|\, \lambda^{(s)}(y)\, dy + \beta\, \lambda^{(s)}(x) = \text{constant} \tag{7}$$

where the superscript s denotes the steady-state solution. By construction, the steady-state solution of our model corresponds to the spatial equilibrium studied in [5]. Without loss of generality, we restrict the search for a steady-state solution on finite support. Therefore, we can assume that $\lambda^{(s)}(x)$ is centered around $x = 0$ with support $[-b, +b]$. By differentiating Eq. (7) twice with respect to x, Mossay and Picard [5] derived the spatial equilibrium equation as

$$\frac{\partial^2 \lambda^{(s)}(x)}{\partial x^2} + \delta^2\, \lambda^{(s)}(x) = 0\,, \tag{8}$$

where $\delta^2 = 2\tau/\beta$. Taking into account the continuity of the solution at support edges, the steady-state solution is given by

$$\lambda^{(s)}(x) = \begin{cases} C\cos(\delta x) & \text{for } x \in [-b, +b] \\ 0 & \text{for } x \notin [-b, +b] \end{cases}. \tag{9}$$

Now we will be interested mainly in studying solutions that are contained into the invariant manifold $I = 1$. Therefore we can compute the parameters b and the amplitude C as a function of the problem parameters as follows:

$$b = \frac{\pi}{2\delta} = \frac{\pi}{2\sqrt{2}}\sqrt{\frac{\beta}{\tau}}\;; \quad C = \frac{\delta}{2} = \sqrt{\frac{\tau}{2\beta}}\,. \tag{10}$$

Once the steady-state solution is determined we can compute $\bar{V}$ explicitly as a function of the model parameters:

$$\bar{V} = p = \alpha - \frac{\pi}{2\sqrt{2}}\sqrt{\beta\tau}\,. \tag{11}$$

where we define the parameter p that is linked to the stability of the invariant manifold. If $p > 0$ the invariant manifold $I = 1$ is transversely stable. The solution (9) is represented in Fig. 1 for some specific parameter values.

The above steady state, once the parameters α, β, τ have been fixed, has been shown to be unique, see [5], or [6]. The main purpose of this paper is to study the stability of the

steady-state solution of Eq. (9) with respect to the dynamics introduced in Eq. (3).

3. Variational equation for stability

3.1. Symmetries of the problem and relevant function spaces

Before ever starting the calculations of the stability of Eq. (9), some general considerations about the symmetries associated with the problem will simplify the calculations. First of all Eq. (3) is a partial integro-differential equation with two independent variables space (x) and time (t). As with respect to time we may consider functions that are of class $\mathcal{C}^1$ with respect to time. Because time does not appear explicitly in Eq. (3) the equation is an autonomous equation with respect to time so that any time translation of a solution will still be a solution of the problem. In physics, this translates the existence of a Goldstone mode associated with time translation invariance. It also relates to energy conservation in the case of Hamiltonian systems (see Noether's theorem). In our problem, this symmetry can be broken by imposing an initial condition at time $t = t_0$. This is precisely what we will do in the following when computing the stability of the steady-state solution $\lambda^{(s)}$ derived in Eq. (9) in the previous section. As with respect to space, there is no spatial derivative appearing in Eq. (3) so that we can work with spatial functions defined in a Hilbert space (e.g. functions that are squared-integrable). By inspection of the spatial part of Eq. (3) there are two immediate symmetries associated with the problem. The problem is invariant to any spatial translation (if the functions are defined in an unbounded domain) so that there is a Goldstone mode associated with this translational invariance. In addition, another invariance holds by the inversion symmetry ($x \to -x$; $y \to -y$). This last symmetry will allows to separate the stability problem into the computation of even- and odd-eigenfunction sectors of the variational equation [12]. On the ground of physical considerations we will work on finite domains and consider the compact support $[-b, +b]$ of the steady solution $\lambda^{(s)}$ as our spatial domain for the stability analysis. It should recalled that from Eq. (10) there is a direct link between the support on which the steady-state $\lambda^{(s)}$ is defined and the parameters of the problem. Therefore, even if we restrict the stability study to the invariant manifold $I = 1$, we have a family of solution $\lambda^{(s)}$ rather than a unique solution. As we will see in the following the stability of the solutions $\lambda^{(s)}$ is directly related to the parameter b.

3.2. Perturbation of the steady-solutions

The stability of the solutions $\lambda^{(s)}$ can be analyzed by perturbing the solution and writing the corresponding variational equation. In the following we consider a small perturbation parameter ε and $\lambda^{(p)}(x, t)$ the perturbation to the steady-state solution.

$$\lambda(x,t) = \lambda^{(s)}(x) + \varepsilon\, \lambda^{(p)}(x,t). \tag{12}$$

Note that as for $\lambda^{(s)}$, $\lambda^{(p)}$ verifies that $\lambda^{(p)}(-b,t) = \lambda^{(p)}(b,t) = 0$. In order to simplify the notation we can define the following linear functional of λ:

$$L[\lambda] = \alpha \int \lambda\, dx - \tau \int |x-y|\, \lambda\, dy - \beta\, \lambda \tag{13}$$

where the integral extends over the whole spatial domain. By using this notation Eq. (3) can be rewritten as:

$$\frac{1}{k}\frac{\partial \lambda}{\partial t} = \left\{ L[\lambda] - \int L[\lambda]\, \lambda\, dx \right\} \lambda \tag{14}$$

If we insert Eq. (12) into Eq. (14) we get at order ε:

$$\frac{1}{k}\frac{\partial \lambda^{(p)}}{\partial t} = \left\{ L[\lambda^{(p)}] - \int L[\lambda^{(s)}]\, \lambda^{(p)}\, dx - \int L[\lambda^{(p)}]\, \lambda^{(s)}\, dx \right\} \lambda^{(s)} \tag{15}$$

which constitutes the variational equation governing the stability of the steady-state family of solution $\lambda^{(s)}$. In order to solve Eq. (15) we first use the principle of separation of variables:

$$\lambda^{(p)}(x,t) = A(t)\, F(x) \tag{16}$$

By plugging Eq. (16) into Eq. (15) and by separating the time and space functions we get a system of two equations:

$$\dot{A}(t) = k\sigma A(t) \tag{17}$$

$$\left\{ L[F] - \int L[\lambda^{(s)}]\, F\, dx - \int L[F]\, \lambda^{(s)}\, dx \right\} \lambda^{(s)} = \sigma F \tag{18}$$

where the over-doted symbol in Eq. (17) stands for a time derivative. Eq. (18) is an eigenvalue problem for the eigenfunction $F(x)$ with eigenvalue σ. We note that this eigenvalue problem is a Fredholm equation of the second kind and there are several well known techniques for finding the corresponding solution set of these eigenvalues and eigenfunctions [13,14].

3.3. Solution to the eigenvalue problem (even modes)

The right-hand-side of Eq. (18) is a linear operator that commutes with the inversion symmetry operator R:

$$RF(x) = F(-x), \tag{19}$$

therefore by using Schur's lemma [12] we can separate the solution of the eigenvalue problem into even and odd eigenmodes. Let us start with even modes. Because eigenfunctions are defined up to a multiplicative constant we can impose a normalization condition for the even eigenfunctions $F(x)$ so that:

$$\int F\, dx = 1 \quad ; \quad \text{or} \quad \int F\, dx = 0 \quad , \tag{20}$$

The latter case (with the integral equal to zero) is a "pathological" case that can be easily dealt with by noting that it corresponds to a mode that perturbs the solution by staying inside the invariant manifold $I = 1$, see the stability of the invariant manifold in Section 2.1. Let us now deal with the case where the eigenmode is normalized to one. By integrating Eq. (18) over the whole domain and using the normalization condition we readily obtain that:

$$\sigma = -L[\lambda^{(s)}] = -p = -\alpha + b\,\tau = -\alpha + \frac{\pi}{2\sqrt{2}}\sqrt{\beta\,\tau}, \tag{21}$$

where p is the parameter defined in Eq. (11). By inspection we also find the corresponding even eigenfunction:

$$F = \lambda^{(s)}(x), \tag{22}$$

For the even sector of the eigenvalue problem there is a single discrete eigenvalue and the corresponding eigenfunction has the same shape as the steady-state solution $\lambda^{(s)}$. The steady-state solution is linearly stable to even perturbations if:

$$\sigma = -\alpha + b\,\tau = -\alpha + \frac{\pi}{2\sqrt{2}}\sqrt{\beta\,\tau} \;<\; 0, \tag{23}$$

which means that the α term is stabilizing and the β and τ terms are destabilizing. We see that there is a critical size for b, $b^{(c)} = \alpha/\tau$, above which the steady solution is unstable to even perturbations. Therefore, concentrated cities ($b < b^{(c)}$) are stable while dispersed cities ($b > b^{(c)}$) are linearly unstable with respect to even perturbations. It should also be noted that the stability result of even eigenmodes leads to the same conclusions as the stability problem of the invariant manifold $I = 1$ that we have performed in Section 2.1.

3.4. Solution to the eigenvalue problem (odd modes)

Let us now concentrate on the odd sector of the eigenvalue problem Eq. (18). For the odd eigenfunctions $F(-x) = -F(x)$ we have always that:

$$\int F\,dx = 0 \tag{24}$$

and Eq. (18) is reduced to a simpler expression:

$$-\lambda^{(s)}(x)\left\{\tau\int |x-y|F(y)\,dy + \beta F(x)\right\} = \sigma F \tag{25}$$

We look for the solution to Eq. (25) by using a sine Fourier expansion on the compact domain $[-b, +b]$:

$$F(x) = \sum_{n=1}^{+\infty} u_n \sin\frac{n\pi x}{b}. \tag{26}$$

By plugging Eq. (26) into Eq. (25) and by multiplying by $\sin(m\pi x/b)\,(\forall m \in \mathcal{N})$ and then by integrating over the whole domain we straightforwardly get the eigenvalue problem in matrix form:

$$\mathcal{A}_{(m,n)}\,u_n = \tilde{\sigma}\,\delta_{(m,n)}, \tag{27}$$

where $\tilde{\sigma} = b\sigma/\beta$ and an explicit expression for the matrix in term of its indices can be written:

$$\mathcal{A}_{(m,n)} = \frac{-8\,m\,n\,(-1)^{(m+n)}\,(1-4n^2+16m^2-16m^4)}{[16n^4+(1-4m^2)^2-8\,n^2(1+4m^2)](1-4m^2)^2}, \tag{28}$$

At this stage we have transformed the solution of the odd eigenfunction problem into the solution of a "simpler" matrix problem. However, there are two important caveats to this operation. First of all in our case we are computing "improper" eigenfunctions. We will see below that we actually need an infinite sum of modes to converge to the solution. In addition the solution toward which the sum is converging is exiting our initial Hilbert space and we rather need to use Schwartz distributions to describe the "improper" odd eigenfunction space. Plainly said, the Hilbert space is too narrow to contain the continuous spectrum of the odd-eigenvalue problem and we have to extend it to a ridged Hilbert space [14]. After being warned about the meaning of solutions given by Eq. (28), we may still compute them to get an idea of the spatial structure of odd eigenfunctions. As an illustration,

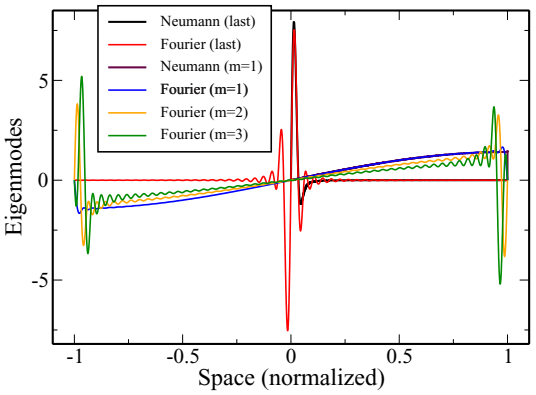

Fig. 2. Approximate odd eigenmodes computed by two methods. (a) By using the Fourier sine expansion with $N = 50$ ($m = 1$ is the mode with $\tilde{\sigma} \to 0$) with the last one corresponding to the mode with $\tilde{\sigma} \to -\pi/4$. (b) By using the Neumann series to avoid the Gibbs phenomenon related to the Fourier expansions [13]; here only the first ($m = 1$) and last modes (least and most stable) are shown. The spatial support is normalized between [1,1].

we set the matrix dimension to $N = 50$ and solve numerically the eigensystem given by Eq. (28) and then reconstruct the $N = 50$ eigenmodes associated with the problem by using Eq. (26) where the upper limit of the sum is now restricted to N. Fig. 2 depicts the odd eigenmodes computed by two different methods, first by the Fourier method (using an expansion of $N = 50$ terms) and second by the Neumann series method which is a classical method to compute the solution of an integro-differential equation (Fredholm second kind) [13]. The Neumann method is an iterative method for solving integral equations that only gives the mode with the largest (in modulus) eigenvalue. This method is reminiscent to the power method that is used in algebra to extract the largest eigenvalue of a matrix. Like the power method, the Neumann method can be adapted by shifting the spectrum to compute also the smallest eigenvalue. Note that in our numerical calculations we have computed only the odd-eigenmodes for $x > 0$ by using the symmetries of the problem. For the odd-eigensystem sector we have found a "continuous" spectrum of eigenvalues in the range:

$$\tilde{\sigma} \in (-\pi/4;\, 0), \tag{29}$$

or equivalently:

$$\sigma \in \left(-\sqrt{\frac{\beta\,\tau}{2}};\, 0\right), \tag{30}$$

that means that all the eigenvalues associated with the improper eigenmodes are stable (or marginally stable for $\sigma \to 0$). Note that the latter is the least stable eigenmode and we see from Fig. 2 ($m = 1$) that it corresponds to the "approximate" Goldstone mode of translation as expected by our preliminary symmetry considerations. The second and third ($m = 2$ and $m = 3$) modes also provide important informations about where the system is more susceptible to be efficiently perturbed, which is close to the domain boundaries ($x = -b$ and $x = b$) where the perturbations induced by the odd modes are the most dangerous even if they are linearly stable. The most stable odd eigenmode is depicted in Fig. 2 (denoted by the label "last" in the figure). We see that its

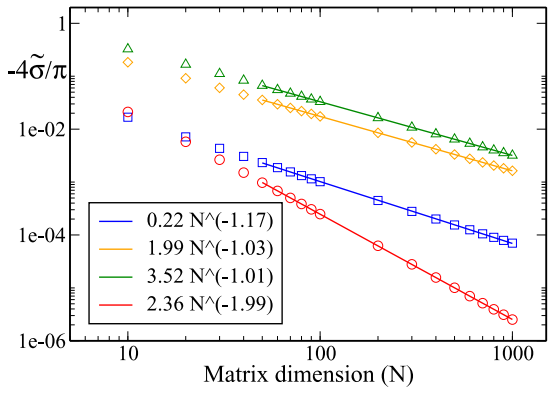

Fig. 3. Convergence of the eigenvalue of the odd eigenvalue problem as a function of the matrix dimension N. The three least stable modes tend to zero (by negative values). The most stable mode tends to $\tilde{\sigma} \to -\pi/4$. In order to show more clearly its convergence rate we have rather plotted $1 + 4\tilde{\sigma}/\pi$ for the last mode. $m = 1$ (blue squares); $m = 2$ (orange diamonds); $m = 3$ (green triangles) ; $m =$ last (red circles). (For interpretation of the references to color in this figure legend, the reader is referred to the web version of this article.)

spatial structure indicates that the perturbation close to the city "center" are the least dangerous for the stability of the steady solution $\lambda^{(s)}$.

Fig. 3 illustrates the rate of convergence of the odd-eigenvalues as a function of the matrix size N. We see that as the matrix dimension increases the density of eigenvalues covering the range $\tilde{\sigma} \in (-\pi/4; 0)$ increases. All these eigenmodes are stable (negative $\tilde{\sigma}$) but they provide interesting information about where the perturbations on the steady solution will be the most dangerous, i.e., near the boundaries of the city. In the next section we illustrate by direct simulation of Eq. (3) all the theoretical results that we have obtained so far.

4. Numerical simulations of the model

In this section we will consider direct numerical simulations of Eq. (3) where the numerical domain is not limited to the support $[-b, +b]$ of the steady state solution. Instead, the perturbation affects a larger support, e.g. a support twice as large as the support that defines the steady state, i.e. $[-2b, +2b]$.

The numerical solution is performed by a straightforward scheme where the time step of integration is set to $dt = 0.001$. We use 401 equidistant spatial points to discretize the support $[-2b, +2b]$ and integrate Eq. (3) by selecting an initial condition at time $t = 0$. All the integrals are evaluated by using Simpson's rule.

4.1. Starting with slightly perturbed steady solutions

Fig. 4 (a–d) illustrate two examples of such simulations. Fig. 4(a) and (b) show the results of the simulation

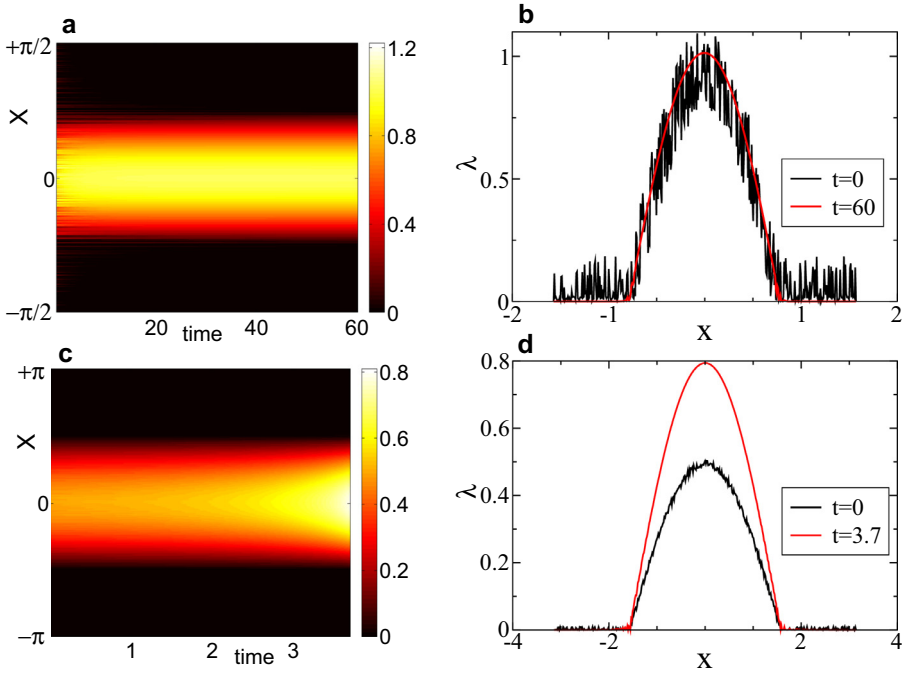

Fig. 4. Numerical simulations for a perturbation active outside the support of the steady state solution, i.e. for $x \in [-2b, +2b]$. (a) Space-time plot of $\lambda^{(s)}(x)$ initially perturbed by a uniform noise $\eta \in (-0.2; +0.2)$ and (b) initial state (black) and final state (red) of the simulation of (a). (c) Space-time plot of $\lambda^{(s)}(x)$ initially perturbed by a uniform noise $\eta \in (-0.01; +0.01)$ and (d) initial state (black) and final state (red) of the simulation of (c). The parameters for simulations (a) and (b) are chosen in the stable region of the invariant manifold ($k = 1$; $\alpha = 1$; $\tau = 1$; $\beta = 1/2$; $b = \pi/4$; $\sigma_{\text{even}} = -p \approx -0.215$). The parameters for simulations (c) and (d) are chosen in the unstable region of the invariant manifold ($k = 1$; $\alpha = 1$; $\tau = 1$; $\beta = 2$; $b = \pi/2$; $\sigma_{\text{even}} = -p \approx 0.57$). (For interpretation of the references to color in this figure legend, the reader is referred to the web version of this article.)

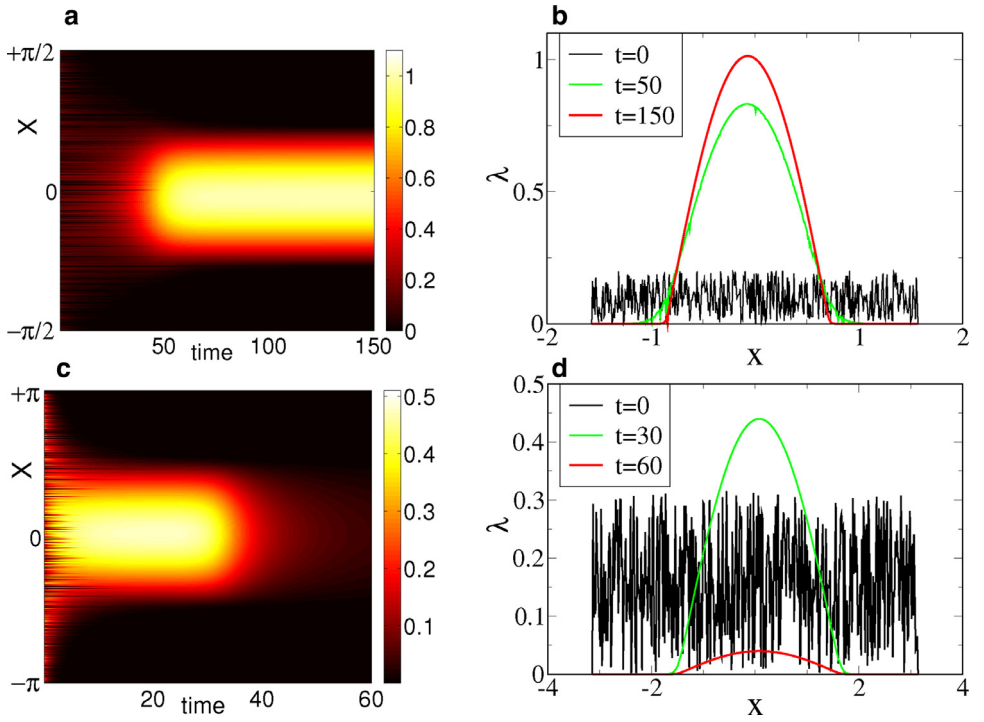

Fig. 5. Numerical simulations starting from uniform noise for $x \in [-2b, +2b]$. (a) Space-time plot of $\lambda(x, t)$ with initial uniform noise $\eta \in (0; +0.2)$ and (b) temporal snapshots of (a) for $t = 0$ (black); $t = 50$ (green); and $t = 150$ (red). (c) Space-time plot of $\lambda(x, t)$ with initial uniform noise $\eta \in (0; +0.3)$ and (b) temporal snapshots of (a) for $t = 0$ (black); $t = 30$ (green); and $t = 60$ (red). The parameters for simulations (a) and (b) are chosen in the stable region of the invariant manifold ($k = 1$; $\alpha = 1$; $\tau = 1$; $\beta = 1/2$; $b = \pi/4$; $\sigma_{\text{even}} = -p \approx -0.215$). The parameters for simulations (c) and (d) are chosen in the unstable region of the invariant manifold ($k = 1$; $\alpha = 1$; $\tau = 1$; $\beta = 2$; $b = \pi/2$; $\sigma_{\text{even}} = -p \approx 0.57$). (For interpretation of the references to color in this figure legend, the reader is referred to the web version of this article.)

when the initial condition is such that the steady solution is stable. To illustrate such a case we have selected the parameters for simulations (a) and (b) to be : $k = 1$; $\alpha = 1$; $\tau = 1$; $\beta = 1/2$; $b = \pi/4$. In that case the even eigenmode has a negative eigenvalue: $\sigma_{\text{even}} = -p \approx -0.215$. We see that the initially perturbed solution is pushed back to the corresponding steady solution Eq. (9) by the relocation dynamics.

On the contrary, if we select the parameters for simulations (c) and (d) to be : $k = 1$; $\alpha = 1$; $\tau = 1$; $\beta = 2$; $b = \pi/2$. The even eigenmode has a positive eigenvalue: $\sigma_{\text{even}} = -p \approx 0.57$ and even if the perturbations added to the steady solution are order of magnitudes smaller than in the case of Fig. 4(a) and (b), we see in Fig. 4(c) and (d) that Eq. (9) is unstable and we also observe that the most dangerous eigenmode (even) has the same shape as the steady solution. Fig. 4(c) shows that a slight perturbation of $\lambda^{(s)}(x)$ leads to a blow up of the solution in finite time as also illustrated in Fig. 4(d).

4.2. Starting from uniform random noise

Let us now use our numerical solver to study the evolution of an initial uniform random noise. Fig. 5(a) and (b) show the results of the simulation when the parameters are selected in the stable region of the steady solution (same parameters as for Fig. 4(a) and (b)). Fig. 5(a) and (b) illustrates that the initial noise is conditioned to evolve through the dynamics to the steady solution. The time scale associated to the evolution to the steady solution is related to the intensity of the initial random noise.

Fig. 5 (c) and (d) show the results of the simulation when the parameters are selected in the unstable region of the steady solution (same parameters as for Fig. 4(c) and (d)). In this case the steady solution is unstable but if we select carefully the initial noise intensity such that the initial noise is almost on the invariant manifold $I = 1$ (but slightly below it). We observe in Fig. 5(c) and (d) that during some transient we can observe the steady solution but the latter is unstable and finally vanishes. If we had selected (not shown) the initial noise such that $I > 1$ the simulation would blow up in finite time as it was the case in Fig. 4(c) and (d).

4.3. Initial "twin" cities

To end up with these simulation examples of Eq. (3) we consider an initial condition with two cities that locate next to each other. As already shown by Mossay and Picard [5], this is not a steady-state solution of the model. Here, we will illustrate the instability of this initial condition and the convergence to the stable unique steady solution. Here, we have taken the same parameters as for Fig. 4(a) and (b). The initial condition is normalized to be on the invariant manifold and we see in Fig. 6(a) and (b) that the system evolves rapidly towards the center between the two cities

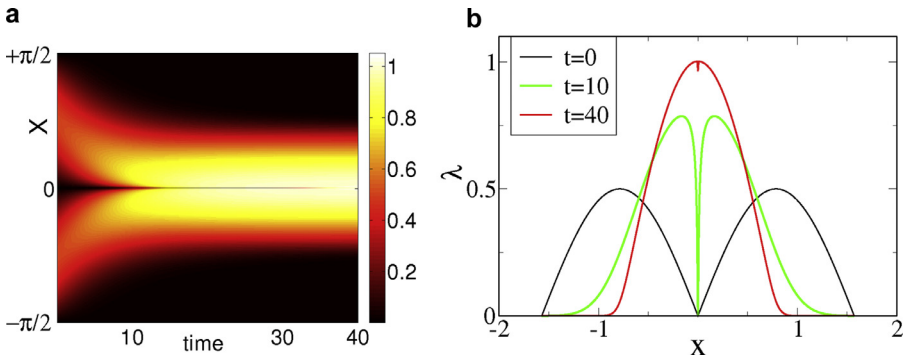

Fig. 6. Numerical simulations starting from "twin" cities for $x \in [-2b, +2b]$. (a) Space-time plot of $\lambda(x, t)$and (b) temporal snapshots of (a) for $t = 0$ (black); $t = 10$ (green); and $t = 40$ (red). The parameters are chosen in the stable region of the invariant manifold ($k = 1$; $\alpha = 1$; $\tau = 1$; $\beta = 1/2$; $b = \pi/4$; $\sigma_{\text{even}} = -p \approx -0.215$). (For interpretation of the references to color in this figure legend, the reader is referred to the web version of this article.)

and forms a single city that corresponds to the steady-state solution.

5. Conclusions

We have extended Beckmann's spatial model of social interactions to a dynamic setting by introducing relocation dynamics. This allows us to study the stability of spatial equilibrium. We have studied the variational equation associated to the stability of the steady solution. We have shown that the even eigenmode sector can be stable or unstable depending on the system parameters. We have also shown that the odd eigenmode sector is always stable. There is a marginal mode in the odd eigenmode sector that is associated with a Goldstone mode (uniform spatial translation of the whole system). All our stability results have been illustrated and confirmed by direct numerical simulations.

Acknowledgments

J.B. acknowledges the financial support by MICINN (Spain) through Grant no. FIS2011-28820-C02-02. The authors wish to thank the two anonymous referees as well as Prof. J. Vanneste (Edinburgh) for valuable suggestions and comments on a previous version of the manuscript. This work has benefited from the support of the COST Action IS 1104.

References

[1] Fujita M, Krugman PR, Venables A. The spatial economy cities, regions and international trade. Cambridge, Mass.: MIT Press; 1999.
[2] Glaeser E, Scheinkman J. Non-market interactions. In: Dewatripont M, Hansen LP, Turnovsky S, editors. Advances in economics and econometrics: theory and applications, eight world congress. Cambridge (UK): Cambridge University Press; 2003. p. 339–69.
[3] Beckmann MJ. Spatial equilibrium in the dispersed city. In: Papageorgiou Y, editor. Mathematical land use theory. Lexington, MA: Lexington Books; 1976. p. 117–25.
[4] Fujita M, Thisse J-F. Economics of agglomeration: cities, industrial location, and regional growth. Cambridge University Press; 2002.
[5] Mossay P, Picard PM. On spatial equilibria in a social interaction model. J Econ Theory 2011;146(6):2455–77. doi:10.1016/j.jet.2011.06.009.
[6] Blanchet A, Mossay P, Santambrogio F. Existence and uniqueness of equilibrium for a spatial model of social interactions. Int Econ Rev [in press]
[7] Ikeda K, Akamatsu T, Kono T. Spatial period-doubling agglomeration of a core-periphery model with a system of cities. J Econ Dyn Control 2012;36:754–78.
[8] Castro S, Correia-da Silva J, Mossay P. The core-periphery model with three countries and more. Pap Reg Sci 2012;91(2):401–18.
[9] Mossay P. Increasing returns and heterogeneity in a spatial economy. Reg Sci Urban Econ 2003;3:419–44.
[10] Mossay P. A theory of rational spatial agglomerations. Reg Sci Urban Econ 2003;43:385–94.
[11] Picard PM, Tabuchi T. Self-organized agglomerations and transport costs. Econ Theory 2010;42:565–89.
[12] Friedman B. Principles and techniques of applied mathematics. New York: Dover; 1956.
[13] Arfken G. Mathematical methods for physicists. Boston: Academic Press; 1985.
[14] Blanchard P, Bruning E. Mathematical methods in physics. Boston: Birkhauser; 2015.